A versatile SLM-enabled atomtronic device for quantum simulation in 2D

T. A. Haase,[1, a)] D. H. White,[1] D. J. Brown,[1] I. Herrera,[1] and M. D. Hoogerland[1]
Dodd-Walls Centre for Photonic & Quantum Technologies, Department of Physics, University of Auckland, Private Bag 92019, Auckland, New Zealand

We report on the implementation of a novel optical setup for generating high-resolution customizable potentials to address ultracold bosonic atoms in 2D. Two key features are developed for this purpose. The customizable potential is produced with a direct image of a spatial light modulator, conducted with an in-vacuum imaging system of high numerical aperture. Custom potentials are drawn over an area of 600×400 μm with a spot-size of 1 μm. The second development is a two-dimensional planar trap for atoms with an aspect ratio of 900 and spatial extent of Rayleigh range 1.6×1.6 mm, providing near-ballistic in-planar movement. We characterize the setup and present a brief catalog of experiments to highlight the versatility of the system.

arXiv:1702.01860v1 [quant-ph] 7 Feb 2017

I. INTRODUCTION

Quantum simulation is an active area of research in which the behavior of complex quantum systems is modeled by simpler, more controllable physical systems[1–4]. For instance, the wave propagation of electrons in a solid, which determines the electrical properties of materials, can be modeled by the wave propagation of ultracold atoms sourced from a Bose-Einstein Condensate (BEC)[5,6]. Such atoms are cold enough that their thermal de Broglie wavelength is larger than the wavelength of visible light, allowing optical structures to be created with similar dimension to the thermal wavelength. This allows for the dynamics of complex systems to be investigated by studying the motion of ultracold atoms in an analogous optical potential. The high degree of controllability inherent in ultracold atom systems means that the dynamical effects of additional layers of complexity can be systematically studied.

These potentials to manipulate neutral atoms are commonly produced by the off-resonant AC Stark shift, which is proportional to the light intensity. Gradients in the light intensity hence generate a force, referred to as the 'dipole force'. Arbitrary potentials can be generated by spatial light modulators (SLMs) which manipulate the phase of the light[7], digital mirror devices (DMDs)[8,9], or by 'painting' time-averaged potentials[10,11]. Hence, the 'programming' on such quantum simulators is performed through the creation of customizable optical potentials to create a Hamiltonian engineered to mimic the desired system.

Application of these light-shaping methods has allowed for the control of cold atoms on varying length scales. On one hand, careful preparation of single atoms on latices has been achieved[12]. On the other hand, novel trap geometries have led to the advent of atomtronics, where atomic analogues of electronic circuits are created. Geometries such as ring traps have been successful in modeling atomic SQUID circuits[13–19], and further trap geometries have been proposed[20–24] and realized[25–27] for other atomtronic circuits.

Here we describe our system used to manipulate ultracold ^{87}Rb atoms trapped in two dimensions. We implement a large area 2D trap which prevents motion in the vertical direction while allowing near-ballistic motion within the plane. At the same time we project customizable light patterns created by an SLM using intensity modulation. The imaging system developed for the SLM is designed to produce optical structures with a resolution of 1 μm. The SLM is imaged using 532 nm light, which produces a repulsive potential for ^{87}Rb. The combination of both these elements allows us to investigate transport dynamics at large length scales in two dimensions which is a region not yet addressed by existing ultracold atom experiments. The ultimate goal of this setup is to move towards a quantum simulator for transport experiments in 2D disordered ultracold atom systems[28].

II. CUSTOMIZABLE POTENTIALS FOR ATOMS

We create customizable potentials by shaping the light field of a 532 nm laser using a Holoeye LC-R 720 SLM. The display is a reflective liquid crystal on silicon (LCoS)[29] chip with a resolution of 1280×768 pixels. Each pixel has a pitch of 20 μm and is addressed using an 8-bit grayscale value. We modulate the light field in intensity, which we find yields images superior to those achievable by phase modulation holography[30–32]. Each pixel of the SLM acts as an adjustable wave plate, which translates to an adjustable intensity through the use of a polariser. The image quality is determined by the quality of the incident beam and induced aberrations from optics.

For our experiments we desire an imaging system capable of producing optical structures of comparable size to the atomic de Broglie wavelength, which is on the order of 1 μm. This will enable a range of experiments, including exotic lattices[33,34], and will tie in with our future aim of studying disordered systems in 2D.

To obtain the resolution required, we position a high numerical aperture (NA) lens inside the main vacuum chamber. The location of the magneto optical trap (MOT) beams place an upper bound on the numerical aperture of the imaging lens. We use an aspheric lens with a NA of 0.42 (Edmund Optics part number 67-278)

[a)] Electronic mail: thaa191@aucklanduni.ac.nz

as the final imaging lens inside the chamber. We designed a lens mount to hold the asphere in place inside the vacuum chamber, primarily under gravity, with minimal surface contact. The lens mount is connected to a custom vacuum flange which in turn is attached to edge welded bellows, as shown in Fig. 1. Extending and contracting the bellows controls the vertical position and tilt of the lens inside the vacuum chamber providing a 20 mm travel length to position the final image in focus with the cold atom cloud.

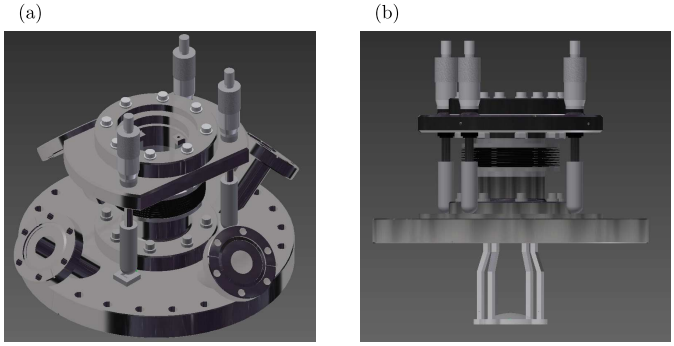

FIG. 1. (a) CAD view of the complete assembly connected to the top 10" flange of the main vacuum chamber. (b) Side view of the CAD assembly showing the lens mount and mounting rods connecting to the bellows. The rods are designed such that when the bellows are at half of the maximum compression, the lens is in focus with the center of the vacuum chamber.

We directly image the face of the SLM with the lens configuration shown in Fig. 3. The SLM is illuminated with up to 5 W of 532 nm light, sourced from a Spectral-Physics Millenia laser, that passes through a polarizing beam splitter after being expanded to a diameter of 32 mm, illuminating the whole SLM screen. Light that is then shifted in polarization, depending on the pixel configuration of the SLM, is imaged by a matched achromat set creating an intermediate image with a magnification of 0.15×. The light is then imaged onto the plane of the atoms using a 250 mm achromat lens and the 0.42 NA asphere, providing a total magnification of 0.036×. With this magnification, we obtain a maximum potential depth for ^{87}Rb of 2.5 μK.

The resolution of the SLM imaging system is measured outside of the vacuum system prior to installation. A vacuum chamber window was also present in the test setup to mimic the working conditions of the system as close as possible. We use two small 3 × 3 pixel squares separated by a set gap (shown in Fig. 2). The gap can be resolved for a 2 pixel gap size placing a lower bound on our resolution of 1 μm, which is the target resolution for our experiments.

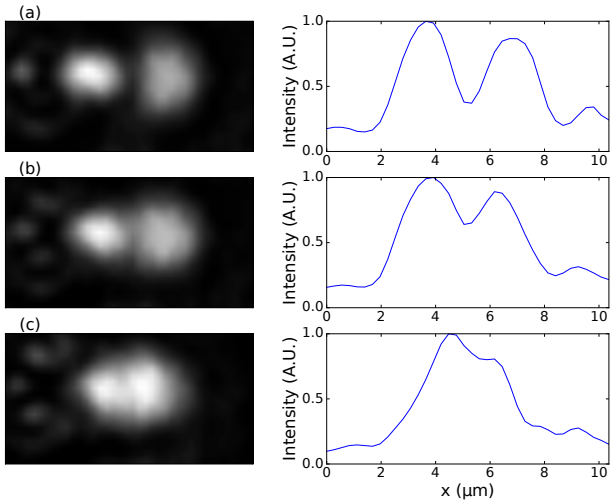

FIG. 2. Two small squares of 3× 3 pixels (2.1 × 2.1 μm) separated by a varying gap (a) 3 px separation (b) 2 px separation (c) 1 px separation with there respective plots summing over the vertical dimension. Images are taken with a CCD camera using a high numerical aperture (40×) microscope objective. The gap between both structures is resolvable for the 2 px separation but not apparent for the 1 px separation.

III. 2D DEGENERATE QUANTUM GAS PRODUCTION

The 2D trap is created by two highly elliptical beams with a wavelength of 1064 nm and an aspect ratio of 16:3 incident at relative angle of 6°, as shown in Fig. 3. The 1064 nm light is sourced from a Nufern 15 W fiber amplifier (NUA-1064-PB-0015-C0), seeded by a Eagleyard 1064 nm diode laser (EYP-RWS-1064-00080-1500-SOT02-0000).The resulting interference pattern creates sheets of light with a spacing of 8 μm. Each of these light sheets provide weak trapping in the x and y dimensions with trap frequencies of 1 Hz. At the same time the trap provides a strong confinement in the vertical z dimension with a frequency of 810 ± 15 Hz. The interference fringes are stable over long periods of time, Fig. 4 shows the fringe shift to be less than 15° over 1 hour, with minimal parametric heating losses. Each fringe has a large spatial extent with a Rayleigh range of 1.6 mm. The main fringe has a trap depth of 2 μK × k_b. This spatial range enables our experiment to observe transport effects in disordered systems that are characterized by spatial lengths on the order of 200 μm or larger. The ratio $\hbar\omega_z/k_bT = 4.8$ shows that vertical excitations are minimal and atoms trapped in the plane are in a 2D regime.

The 2D degenerate gas of ultracold atoms is generated by loading an initial Bose-Einstein condensate (BEC) into the 2D trap. Our vacuum chamber setup and BEC generation is described in earlier work[35], with the addition of a 2D MOT. In brief, a 2D MOT loads the 3D MOT located inside the main ultra-high vacuum chamber. An

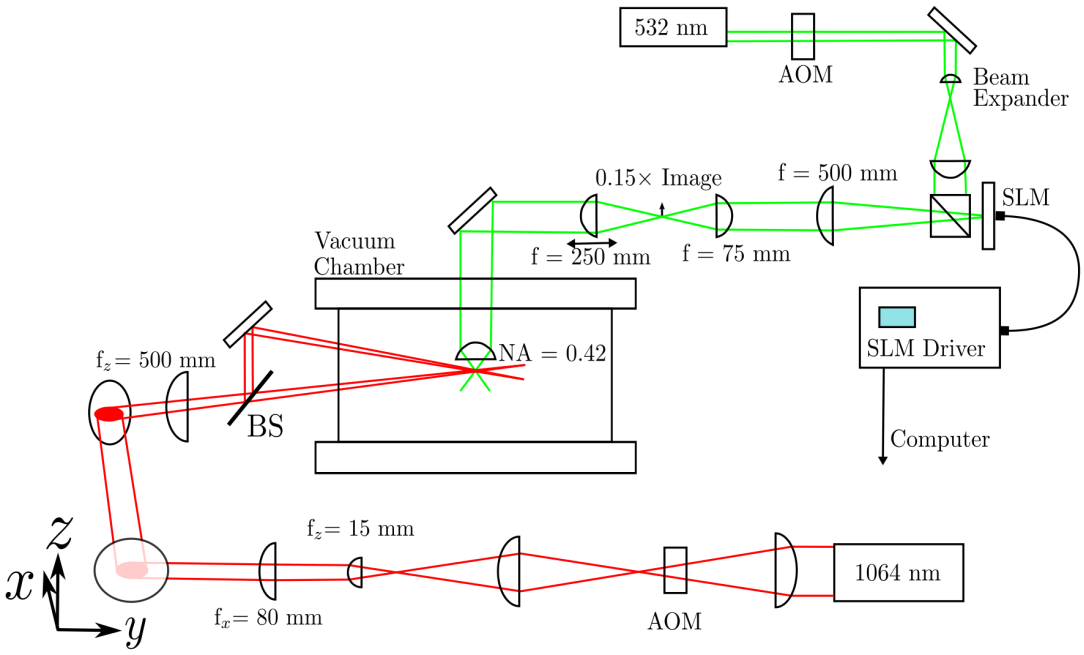

FIG. 3. Overview of the optical setup showing the focal lengths and positions of lenses used. The 532 nm light that is used to illuminate the SLM is shown in green. Positioning of the lens inside the vacuum chamber is controlled by bellows (not drawn). The f = 250 mm lens before the chamber is placed on a translation stage for fine control of focusing. An intermediate image between the f = 500 mm lens and the f = 250 mm lens is created with 0.15× magnification. The 1064 nm light used to produce the 2D trap is shown in red. The beam, emitted by a fiber laser, is power controlled using an AOM . The beam is expanded and then shaped using two collimating cylindrical lenses, the first of 15 mm in focal length in z and then a 80 mm focal length in x. The resultant beam is collimated and highly elliptical with an aspect ratio of 16:3 (x:z). The beam is then angled 3° upwards and passes through a weak cylindrical lens with focal length of 500 mm in z. A plate beamsplitter (BS) splits the beam creating a vertical beam that is then reflected to intersect the lower beam. Both beams focus and intersect on the atoms creating the 2D trap.

all-optical ^{87}Rb BEC is produced by evaporatively cooling atoms, optically pumped to the $|F = 1, m_F = -1\rangle$ state, loaded into a crossed-beam CO_2 dipole trap.

Loading of the 2D planar trap begins following the production of the BEC. The ramp sequence is shown in Fig. 6. In the first section of the ramp the 1064 nm beams are linearly ramped up to full power in 1000 ms, while the CO_2 beams are simultaneously ramped down to 20% of the power at Bose-Einstein condensation. All laser powers are maintained at this power for 100 ms to equilibrate the system, with the CO_2 beams providing weak radial confinement and the 1064 nm beams providing suspension against gravity. The CO_2 beams are subsequently ramped down to zero in 20 ms, which releases the atoms into the 2D trap. Using this loading scheme we obtain a loading efficiency of $70 \pm 1\%$ into the 2D trap.

We now characterise the behavior of the 2D degenerate gas of ultracold atoms inside the 2D trap. After the atoms are loaded into the 2D trap they are left to expand. Fig. 5(a–c) shows the atoms expanding inside the 2D trap for different expansion times. We measure the atomic radius at different expansion times and observe a linear increase of the radius over a time period greater than 100 ms, with the plot shown in Fig. 5(d). The linear growth of the atomic radius indicates ballistic expansion. By applying a linear fit to the data we obtain a temperature of 8 nK for the atoms corresponding to a de Broglie wavelength of 2 μm. We measure a trap lifetime of 2 s. It should be stressed that any heating due to vibrations or otherwise will cause the atoms to escape from the trap, which has a shallow trap-depth under gravity of 2 μK.

IV. IMAGING

During the CO_2 laser ramp-down, the 532 nm light is ramped to full power simultaneously. The 532 nm light projects the desired potential onto the atoms. In this section we show some example experiments which reflect the control over atoms which the setup provides. In these experiments, the atoms begin from a point source at the location of the CO_2 beam intersection. A visualization of the location of all 3 beams and intensity ramps is shown in Fig. 6. With blue-detuned light, a clear method is to

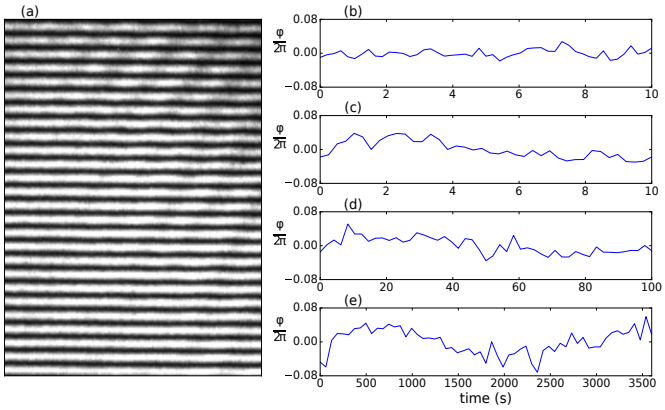

FIG. 4. (a) Image of the fringes generated by the interfering 1064 nm elliptical beams. The fringes are monitored over time and fitted with a cosine fit where we plot the change in phase taking an image every (b) 200 ms for 10 s (c) 200 ms for 10 s with a source of acoustic noise, namely the finale of Tchaikovsky's 1812 Overture played at 80 dB (d) 2 s for 100 s and (e) 60 s for 36000 s.

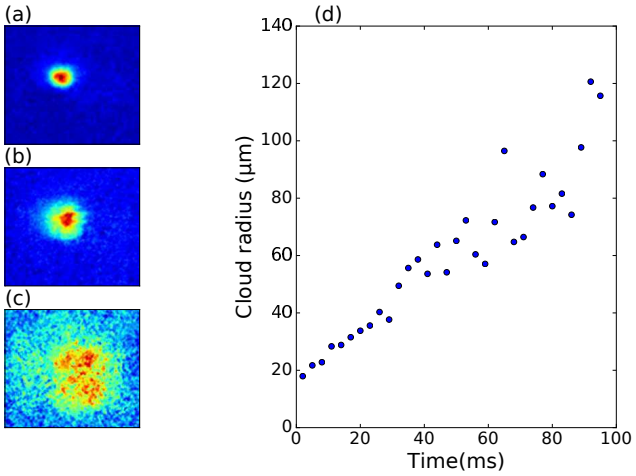

FIG. 5. Expansion of the atoms in the 2D trap. Images of the atoms taken after (a) 8 ms, (b) 20 ms and (c) 50 ms expansion times averaged over 3 experimental runs.The atomic cloud profiles are fitted with Gaussian functions from which the atomic radius is extracted. The atomic radius is plotted with time (d) for 100 ms of total expansion. The linear increase of the radial size shows ballistic expansion of the cloud in the 2D trap.

image the outline of a certain shape and allow the atoms to expand to fill the void. This is different from other experiments where the atoms are evaporated in the presence of the potential taking on the shape of the projected image[8]. As such, our experiments are transmissive and require a defined path for the atoms to expand into.

Figure 7 shows an image of atoms where the outline of a kiwi bird has been imaged onto the plane. The general outline is well resolved, while the 'beak' and 'feet' are partially resolved due to the small size in channel width

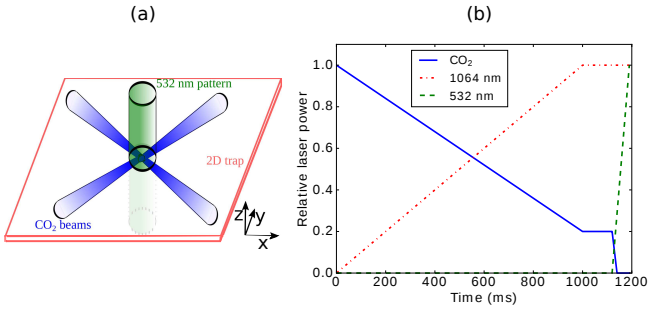

FIG. 6. (a) Representation of the intersection of all 3 beams; the CO_2 beams (blue); 1064 nm planar trap (red); and 532 nm SLM generated pattern (green). In this case the pattern imaged is a hollow cylinder. (b) Beam intensity ramps for all 3 beams during the loading process and application of the tailored potential. A relative laser power of 1 corresponds to an output of 50 mW for the CO_2 laser, 8 W for the 1064 nm laser and 3 W for the 532 nm laser.

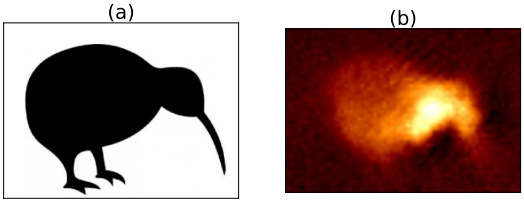

FIG. 7. Atoms taking on the shape of a kiwi-bird potential, which is 150 μm head to tail. (a) Image of the kiwi shown on the SLM (b) Image of atoms inside the kiwi potential after 300 ms of expansion averaged over 20 experimental runs.

of approximately 5 μm, limiting the flow of atoms into these structures.

We can also look at more functional geometries to analyze atomic transport dynamics. A 'dumbbell' structure, where an initial circular reservoir loaded with the atoms is connected by a channel to a secondary reservoir, allows for a controlled study of transmissive experiments for where the chemical potential drives the atoms from one reservoir to the other. Figure 8 shows the expansion of the atoms into a such a potential with a 35 μm long channel after 150 ms of expansion time. We define the number imbalance as

$$\Delta N = \frac{N_i - N_f}{N_i + N_f}, \tag{1}$$

where N_i is the atom number in the initial reservoir and N_f of the final reservoir. Dumbbell structures create a double-well structure which can be used to model a range of systems. For example, dumbbell geometries have been used to model a resistor-capacitor-inductor (RCL) atomtronic circuit[24,27,36]. We create the dumbbell using the SLM, allowing the channel width and length to be tailored to investigate the atom transport. The data in

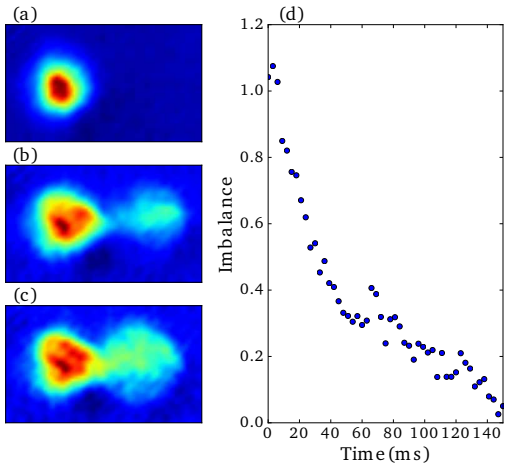

FIG. 8. (a) Initial loading of atoms into a single reservoir on the left-hand-side of the 'dumbbell' shape. The channel length is 35 μm and the width is 30 μm. The reservoir radii are 35 μm. (b) Expansion of the atoms inside the trap after 45 ms. (c) Atoms loading into the secondary reservoir of the dumbbell after 120 ms (d) Plot of number imbalance between both reservoirs in time.

Fig. 8(d) shows the atom number imbalance against time. Two transport regimes are observed. The first 40 ms are dominated by ballistic transport, resulting in a rapid linear decrease of the imbalance. Once a sufficient number of atoms have entered the second reservoir the effects of the chemical potentials dominate the transport. We observe an exponential decay coupled with oscillatory behaviour. In this regime the system is best modelled by the above RCL atomtronic circuit. This model predicts oscillatory behaviour and energy exchange between the chemical potential of the reservoirs and the kinetic energy of the atoms, at a frequency determined by $\omega = 1/\sqrt{LC}$.

In future experiments, adding disorder to the channel opens up the possibility of studying localization effects. The long spatial range of our experiment will also allow us to study length scales comparable to that of localization lengths for cold atom systems.

Other geometries can be used, such as ring traps, as shown in Fig. 9. Here atoms are initially loaded onto the left-side of a 70 μm outer diameter ring and allowed to expand. Ring traps have proven to be a test bed for numerous quantum effects[37]. Moreover, there is the possibility to use rings as atomtronic systems by analyzing the atom number imbalances in the left and right side of the ring[16].

V. SUMMARY

To summarize, we have presented an ultracold atom setup capable of conducting transport experiments over large length ranges in 2D. Customizable repulsive potentials are generated by a SLM using intensity modulation

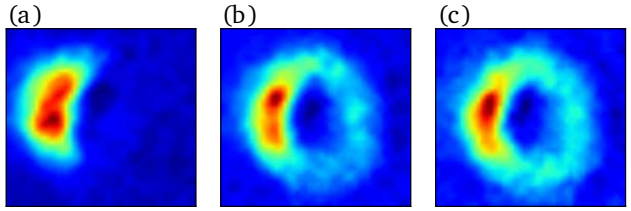

FIG. 9. Atoms expanding into a ring potential. The inner diameter of the ring is 60 SLM pixels and the outer diameter is 120 SLM pixels. The atoms are shown at different expansion times of (a) 0 ms (b) 50 ms (c) 100 ms.

to shape the light field of a 532 nm laser. An imaging system, with a lens inside the ultra high vacuum chamber, is used to generate optical potentials with a lower-bound resolution of 1 μm. Our initial results with a variety of geometries demonstrate the versatility of our setup. Our system provides a test bed for experiments on quantum transport and localization. Furthermore, results leading into atomtronics have also been observed.

VI. ACKNOWLEDGMENTS

We gratefully acknowledge the support of the Marsden Fund, with funding administered by the Royal Society of New Zealand.

[1] I. Bloch, J. Dalibard, and S. Nascimbène, Nat. Phys. **8**, 267 (2012).
[2] P. J. J. O'Malley *et al.*, Phys. Rev. X **6**, 031007 (2016).
[3] J. I. Cirac and P. Zoller, Nat. Phys. **8**, 264 (2012).
[4] B. P. Lanyon *et al.*, Science **334**, 57 (2011).
[5] C.-C. Chien, S. Peotta, and M. Di Ventra, Nat. Phys. **11**, 998 (2015).
[6] J. Billy, V. Josse, Z. Zuo, A. Bernard, B. Hambrecht, P. Lugan, D. Clément, L. Sanchez-Palencia, P. Bouyer, and A. Aspect, Nature **453**, 891 (2008).
[7] P. Zupancic, P. M. Preiss, R. Ma, A. Lukin, M. E. Tai, M. Rispoli, R. Islam, and M. Greiner, Opt. Express **24**, 13881 (2016).
[8] G. Gauthier, I. Lenton, N. M. Parry, M. Baker, M. J. Davis, H. Rubinsztein-Dunlop, and T. W. Neely, Optica **3**, 1136 (2016).
[9] C. Muldoon, L. Brandt, J. Dong, D. Stuart, E. Brainis, M. Himsworth, and A. Kuhn, New Journal of Physics **14**, 073051 (2012).
[10] K. Henderson, C. Ryu, C. MacCormick, and M. G. Boshier, New Journal of Physics **11**, 043030 (2009).
[11] T. A. Bell, J. A. P. Glidden, L. Humbert, M. W. J. Bromley, S. A. Haine, M. J. Davis, T. W. Neely, M. A. Baker, and H. Rubinsztein-Dunlop, New Journal of Physics **18**, 035003 (2016).
[12] W. S. Bakr, J. I. Gillen, A. Peng, S. Folling, and M. Greiner, Nature **462**, 74 (2009).
[13] A. Ramanathan, K. C. Wright, S. R. Muniz, M. Zelan, W. T. Hill, C. J. Lobb, K. Helmerson, W. D. Phillips, and G. K. Campbell, Phys. Rev. Lett. **106**, 130401 (2011).
[14] K. C. Wright, R. B. Blakestad, C. J. Lobb, W. D. Phillips, and G. K. Campbell, Phys. Rev. A **88**, 063633 (2013).

[15]F. Jendrzejewski, S. Eckel, N. Murray, C. Lanier, M. Edwards, C. J. Lobb, and G. K. Campbell, Phys. Rev. Lett. **113**, 045305 (2014).
[16]S. Eckel, J. G. Lee, F. Jendrzejewski, N. Murray, C. W. Clark, C. J. Lobb, W. D. Phillips, M. Edwards, and G. K. Campbell, Nature **506**, 200 (2014).
[17]D. Aghamalyan, M. Cominotti, M. Rizzi, D. Rossini, F. Hekking, A. Minguzzi, L.-C. Kwek, and L. Amico, New Journal of Physics **17**, 045023 (2015).
[18]Y.-H. Wang, A. Kumar, F. Jendrzejewski, R. M. Wilson, M. Edwards, S. Eckel, G. K. Campbell, and C. W. Clark, New Journal of Physics **17**, 125012 (2015).
[19]A. C. Mathey and L. Mathey, New Journal of Physics **18**, 055016 (2016).
[20]R. A. Pepino, J. Cooper, D. Z. Anderson, and M. J. Holland, Phys. Rev. Lett. **103**, 140405 (2009).
[21]B. T. Seaman, M. Krämer, D. Z. Anderson, and M. J. Holland, Phys. Rev. A **75**, 023615 (2007).
[22]S. C. Caliga, C. J. E. Straatsma, and D. Z. Anderson, New Journal of Physics **18**, 025010 (2016).
[23]S. C. Caliga, C. J. E. Straatsma, A. A. Zozulya, and D. Z. Anderson, New Journal of Physics **18**, 015012 (2016).
[24]J. G. Lee, B. J. McIlvain, C. J. Lobb, and W. T. Hill, III, Sci. Rep. **3**, 1034 (2013).
[25]S. Eckel, F. Jendrzejewski, A. Kumar, C. J. Lobb, and G. K. Campbell, Phys. Rev. X **4**, 031052 (2014).
[26]R. Labouvie, B. Santra, S. Heun, S. Wimberger, and H. Ott, Phys. Rev. Lett. **115**, 050601 (2015).
[27]S. Eckel, J. G. Lee, F. Jendrzejewski, C. J. Lobb, G. K. Campbell, and W. T. Hill, Phys. Rev. A **93**, 063619 (2016).
[28]E. Abrahams, *50 Years of Anderson Localization* (2010).
[29]C. H. Gooch and H. A. Tarry, Journal of Physics D: Applied Physics **8**, 1575 (1975).
[30]R. W. Gerchberg and W. O. Saxtion, Optik **35**, 237 (1972).
[31]M. Pasienski and B. DeMarco, Opt. Express **16**, 2176 (2008).
[32]A. L. Gaunt and Z. Hadzibabic, Scientific Reports **2**, 721 (2012).
[33]G.-B. Jo, J. Guzman, C. K. Thomas, P. Hosur, A. Vishwanath, and D. M. Stamper-Kurn, Phys. Rev. Lett. **108**, 045305 (2012).
[34]L. Tarruell, D. Greif, T. Uehlinger, G. Jotzu, and T. Esslinger, Nature **483**, 302 (2012).
[35]Y. C. Wenas and M. D. Hoogerland, Rev. Sci. Instrum. **79**, 053101 (2008).
[36]A. Li, S. Eckel, B. Eller, K. E. Warren, C. W. Clark, and M. Edwards, Phys. Rev. A **94**, 023626 (2016).
[37]G. D. Bruce, J. Mayoh, G. Smirne, L. Torralbo-Campo, and D. Cassettari, Physica Scripta **2011**, 014008 (2011).